On the Measurement and Modeling of Polymeric Materials that Exhibit Unstable Localized Necking

Ted Diehl

DuPont
DuPont Engineering Technology, Chestnut Run, Bldg 722, Wilmington, DE 19880-0722
Ted.Diehl@USA.DuPont.com

Abstract: Some polymeric materials are known to exhibit localized necking instabilities during uniaxial tension testing. Once the neck begins, it first localizes and then propagates over the length of the sample. After it has fully propagated, the material will often endure significant amounts of additional deformation before complete failure. The localized necking creates a problem in that traditional methods of measuring strain & stress from the sample become invalid. Even the newest imaging correlation methods are unable to properly measure the sample's strain and stress. This paper presents a pragmatic approach to salvage such data and discusses its use within finite element models.

Keywords, Buckling, Constitutive Model, Experimental Verification, Material Instability, Sample Necking, Plasticity.

1. Introduction

Polymeric films are used in a host of structural applications, many of which are related to some form of containment or packaging. In many of these applications, the film endures very large deformations and strains. This may occur during the creation of the structural shape, such as thermoforming, or it may be during its application use, such as the opening of a plastic package. In many cases, material characterization of these films can be quite challenging, especially if the film exhibits localized necking instabilities as it is deformed into the inelastic regime.

Figure 1 shows localized necking developing in a polyamide-based film as it is deformed in a uniaxial tension experiment. The material being evaluated is 0.203 mm thick Ö-Colamin "MP" Flachfolie, a film composed of two polyamide layers and a layer of polyethylene. This particular film, manufactured by Obermühle Polymertechnik, was chosen for this study because it exhibits *initial* isotropic behavior. This means that uniaxial test specimens cut from any orientation of a sheet of material produce essentially the same[1] uniaxial deformation results, even for very large deformations of up to 300% Biot (nominal) strain. The qualifier *initial* implies that as the material

[1] With the acknowledgement that locations of any localized necks can be random, sample to sample.

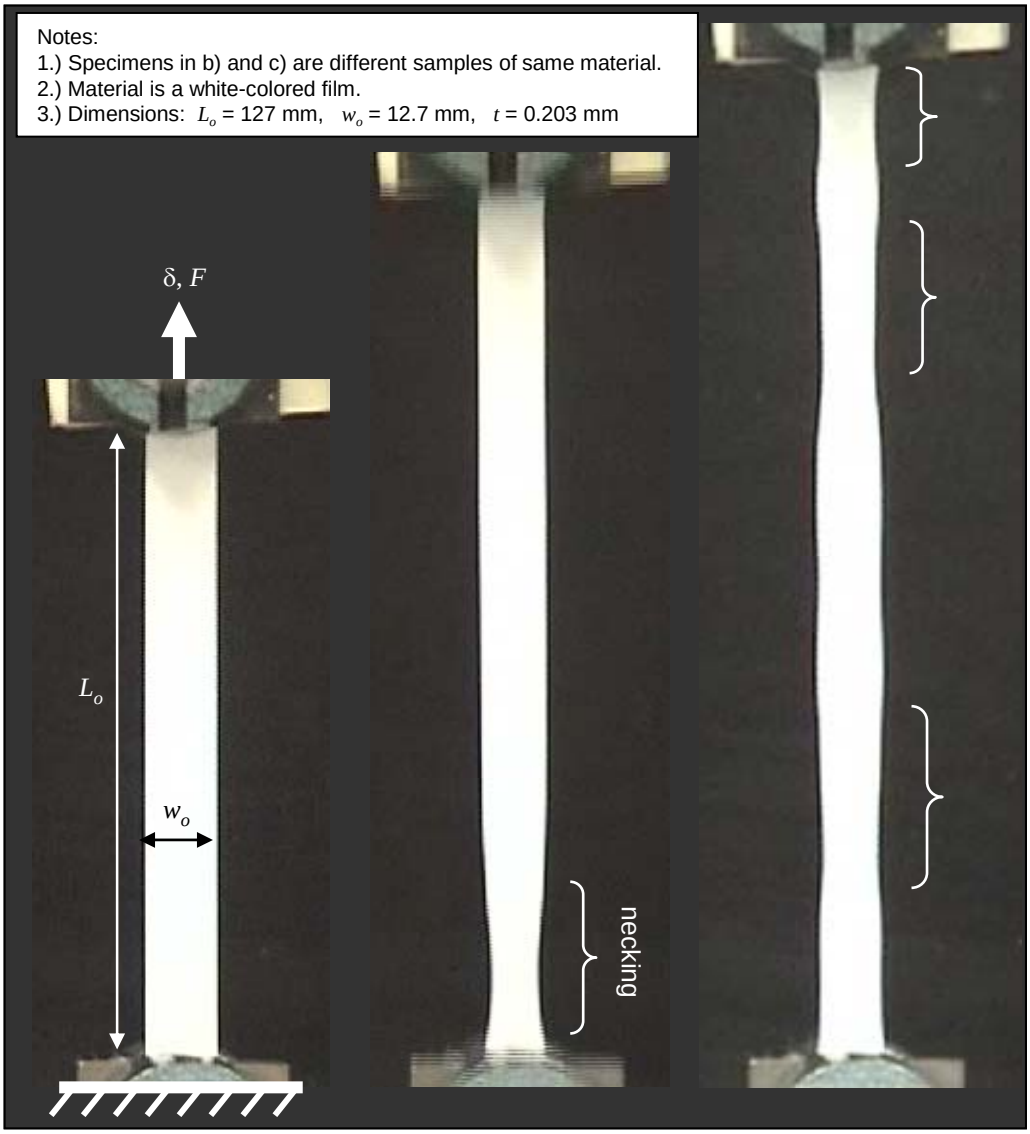

Figure 1: Examples of localized necking in uniaxial tensile tests of Obermühle Ö-Colamin "MP" Flachfiol Film.

is deformed, especially to large strains, the material may not exhibit further isotropic behavior about that deformed state.

Figure 1 displays two of the many specimens that were physically tested in the study. These two specimens (Figure 1b and c) demonstrate that the location of the necking can appear to be random, varying from sample to sample. In particular, Figure 1c shows that necking does not always begin near a clamped boundary.

The necking behavior is a form of instability and thus creates several problems when attempting to analyze such a material:

- What is a viable stress/strain representation for this material?
- Assuming a material representation exists, can this be modeled with finite element methods?

This paper presents a pragmatic approach that can be used to characterize such materials. It further discusses some of the issues that occur when finite element analysis is performed with such unstable materials.

2. Uniaxial loading

While a host of testing methods exist that can evaluate various deformation modes of a material (uniaxial tension/compression, biaxial tension/compression, simple shear, etc.), the uniaxial tension test is by far the most common method utilized for characterizing the structural material behavior of films. Classical uniaxial testing methods would utilize a dog-bone shaped specimen and local strain measurement (via strain gage) in the "narrow section" of the specimen to obtain a uniform strain and stress state, avoiding effects caused by the fixed boundary conditions at the two ends of the specimen. However, when testing polymeric films (in industry), this classical approach is not used because the films endure large strains making it impossible to use traditional strain gages (and adherence and local stiffness of such gages would invalidate any measurement). It is possible to utilize non-contact methods[2] to obtain measurements of the strain in the "narrow section" of the dog-bone over a large range of deformation. However, these methods can be non-trivial and time consuming to utilize, and ultimately too costly for many industrial applications.

The author's industrial experience indicates that the method often implemented for uniaxial testing of polymeric film is ASTM D882 (or variants of this standard). A simple rectangular specimen is used and strains are calculated based on cross-head motion (grip separation). Nominal stresses are calculated from the load applied and the original cross-sectional area of the specimen. To minimize boundary effects caused by the grips at the ends of the sample, a length to width ratio of 10:1 (or greater) should be used. The Biot (nominal) strain during the test is then calculated by measuring the total change in the length of the specimen (between the grips) relative to its original length, L_o, where care must be taken to ensure that grip slip is negligible. For a material obeying

[2] Examples include "laser strain gages" or "digital image correlation" methods such as the *StrainMaster* system (by LaVision) or the *Aramis* system (by GOM).

Hooke's law, the error in estimating its initial elastic modulus using this method is less than 1 %. This is can be demonstrated by comparing the "computed elastic modulus," derived by applying this method to a finite element model, relative to the known elastic modulus used in the model. The key to the validity of this approach is that the stress and strain are uniform over the vast majority of the sample.

2.1 Measures of stress and strain

Regardless of the method used to measure the stress and strain in the sample, distinction must be made between *nominal* measures (based on undeformed cross-sectional area and undeformed gage lengths) and *true* measures (based on deformed geometry) if large strains are expected. This section defines several measures of stress and strain for uniaxial deformations.

The stretch ratio, λ, is simply computed from the current gage length (L) relative to the undeformed gage length (L_o). The volume ratio, J, is defined similarly using deformed and undeformed volumes. Hence we have

$$\lambda = \frac{L}{L_o} \quad \text{and} \quad J = \frac{V}{V_o}. \tag{1a, b}$$

The nominal (Biot) and true (logarithmic) strains are define as

$$\varepsilon_b = \lambda - 1 \quad \text{and} \quad \varepsilon_{\ln} = \ln(\lambda). \tag{2a, b}$$

The nominal, true (Cauchy), and Kirchhoff stress measures are

$$T = \frac{F}{A_o}, \quad \sigma = \frac{F}{A}, \text{ and } \quad \tau = J\sigma. \tag{3a, b, c}$$

where the cross-sectional area is defined by A_o in the undeformed state and A in the deformed state.

When the deformation is small and elastic, the difference in nominal and true measures is negligible and the volume ratio remains near unity. As the deformations increase, then differences in strain and stress measures becomes very noticeable. In many cases we can map between nominal and true measures based on a few assumptions. For polymers, inelastic deformations are approximately incompressible and the elastic component of the deformation remains small, implying that the volume ratio remains near unity for all deformation ranges. Typical work-conjugate pairs are (λ, T) and $(\varepsilon_{\ln}, \tau)$. Noting that these assumptions imply that $J = 1$ over the entire deformation range, this means that $(\varepsilon_{\ln}, \sigma)$ is also work-conjugate. We can also relate the true stress to the nominal stress via

$$\sigma = \lambda \cdot T. \tag{4}$$

2.2 Measuring *apparent* stress/strain data for materials that exhibit localized necking

Figure 2 presents results from a uniaxial tension test of the Ö-Colamin film. The four deformed images are from a single specimen. Figure 2e presents an *apparent* nominal stress/strain curve for the test. This curve denotes various regions such as the onset of necking, steady neck propagation, the onset of neck arresting, the beginning of secondary hardening, and lastly, the point at which no further local necking occurs. If the sample were clamped with ideal clamps such that lateral contraction at the clamp was not constrained, then when necking ran the full length of the sample, secondary hardening would clearly begin and the transition region (as shown) would not exist.

The *apparent* nominal stress data is derived by dividing the applied load with the original cross-section area. The *apparent* stretch ratio is the ratio of the deformed gage length (distance between the grips) relative to the undeformed gage length. The *apparent* nominal strain is *apparent* stretch ratio minus 1. This data is denoted as "apparent" because once the sample begins to neck (state A in Figure 2e), the assumption of uniform deformation over the entire sample is clearly being violated. Technically, the calculations of stress, stretch ratio, and strain between states A and B are invalid.

So the question to answer is "Can the test be performed so that necking does not occur and if not, how can a valid stress/strain curve for the material be obtained?" It is noted that while the location within the specimen of where the localized necking will initiate varies from specimen to specimen (Figure 1), the resulting apparent nominal stress/strain curves from various samples are often very similar. It is further noted that if a dog-bone specimen shape is utilized, then the localized necking will occur in the "narrow section" of the dog-bone, again creating a problem.

It is often suggested that a non-contact digital image correlation method can obtain a proper strain measurement in the necked region, thus providing a way to obtain valid stress/strain data. Unfortunately, this approach is not sufficient for several reasons. Figure 3 depicts local nominal strain contours of a specimen as it initially necks locally and then the neck propagates. This strain data, while resulting from a finite element simulation (to be described later), could equally have come from a non-contact digital image correlation method applied to the physical experiment. In particular, Figure 3b shows that as the neck initially forms, the local strain state in the neck is not uniform across the width of the sample. This implies that the local stress state is not uniform across the sample's width. While it is true that an experimentally obtained strain measurement from an image correlation method might give acceptable strain values, there is no "direct measurement method" to determine the local stress that correlates with that strain. As shown in the simulation results, the local stress is varying across the width of the sample in a non-trivial manner because the local stiffness of the material, which is nonlinearly dependent on its local strain, is varying. Moreover, it would be inaccurate to use the "necked area" as the deformed area to divide into the applied load to obtain a true stress.

Another point to make about evaluating a localized neck is that the strain gradients are very large and the strain in the neck quickly increases to very large values as a function of time. Referring to Figure 3 we see that while the apparent strain is changing slowly from 9.0% to 12.6%, the maximum local strain changed from 9.9% to 108.0%, almost an additional 100% of strain! These large and fast developing strain gradients are difficult to accurately measure experimentally; often

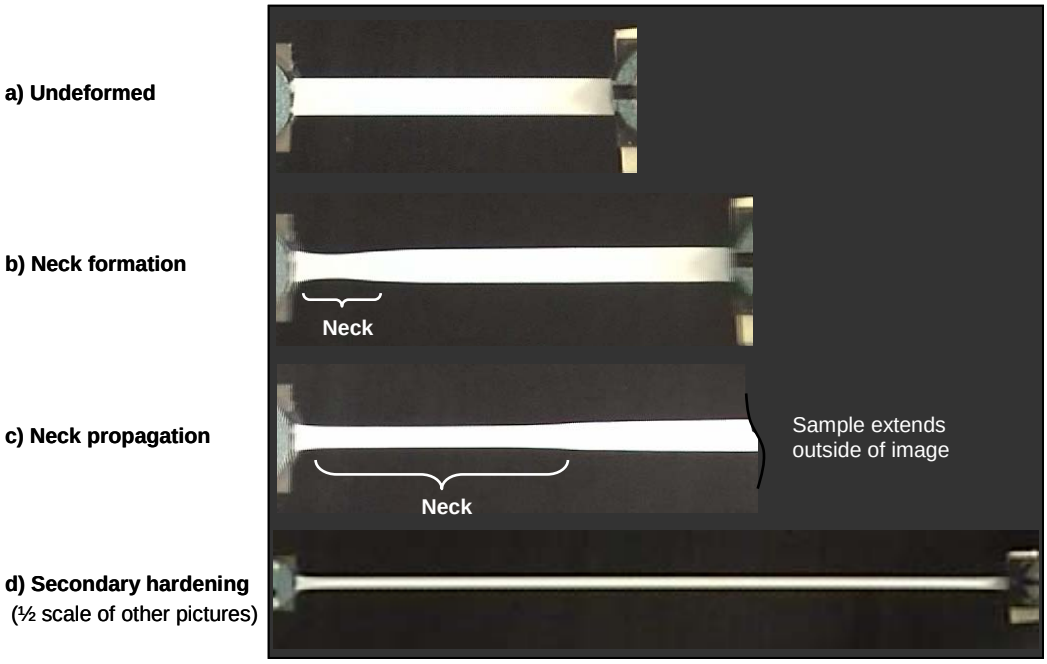

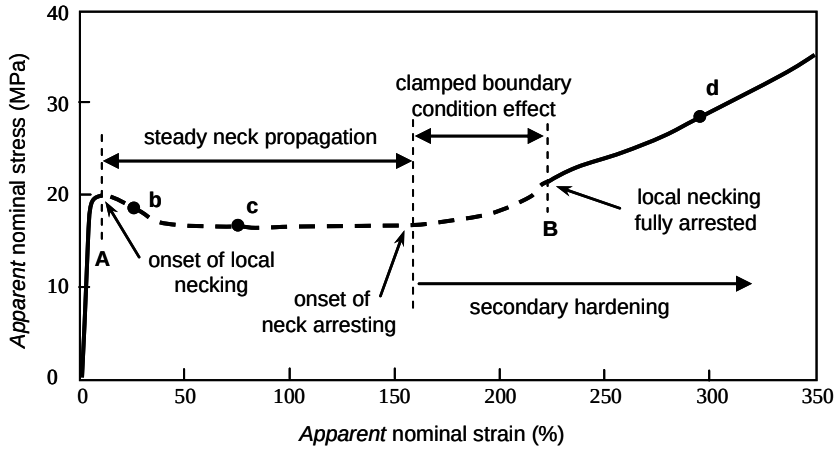

e) *Apparent* nominal stress/strain curve derived from cross-head load and cross-head motion

Figure 2: Figure 2: Assessment of an apparent nominal stress/strain measurement from uniaxial tensile data of Obermuhle O-Colamin Flachfil Film.

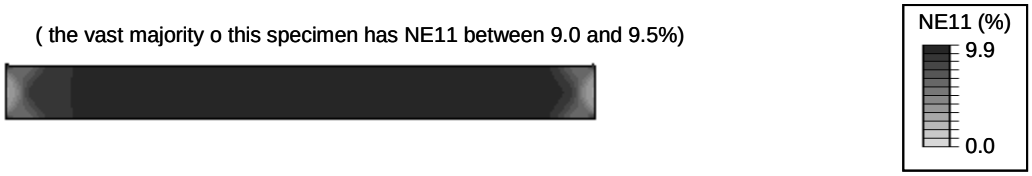

a) Local nominal strain measure NE11 at an apparent nominal strain of 9.0 %

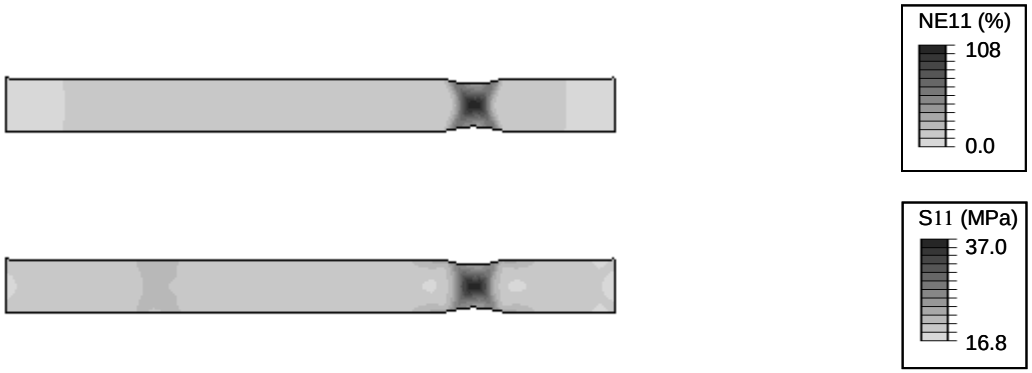

b) Local nominal strain measure NE11 and local true (Cauchy) stress measure S11 at an apparent nominal strain of 12.6 %

c) Local nominal strain measure NE11 at an apparent nominal strain of 34 %

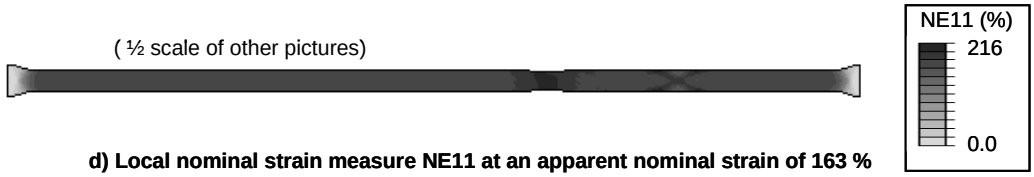

d) Local nominal strain measure NE11 at an apparent nominal strain of 163 %

Figure 3: Depiction of local strain and stress measures as neck develops and propagates.

requiring high resolution, high speed video cameras. This result, coupled with the lack of ability to directly measure the local stress, still leaves us with a set of measured data that would appear to be insufficiently accurate to directly characterize the stress/strain response of the material.

2.3 Uniaxial instability analysis

The onset of necking occurs when the local tangent slope of the nominal stress/strain curve passes zero and becomes negative (state A in Figure 2e). The following analysis, based on formulae published in ABAQUS (1996), is used to develop the criterion for the onset of necking and the regaining of stability if necking becomes arrested. For a specimen under a uniform uniaxial strain state, we repeat our assumption that for polymeric materials the deformation will be approximately volume conserving. This implies

$$A \cdot L = A_o \cdot L_o \,. \tag{5}$$

Noting that the original area and length do not change, we find that differentiating the above produces

$$dA \cdot L + A \cdot dL = 0 \quad \rightarrow \quad dA = -A\frac{dL}{L}. \tag{6}$$

Noting that the derivative of the true strain is $d\varepsilon_{\ln} = dL/L$, we see that

$$dA = -A \cdot d\varepsilon_{\ln} \,. \tag{7}$$

Rearranging and differentiating the true stress formulae of equations 3b, we have

$$dF = A \cdot d\sigma + \sigma \cdot dA \,. \tag{8}$$

Substituting the above results and rearranging obtains

$$\frac{dF}{dL} = \frac{A}{L}\left(\frac{d\sigma}{d\varepsilon_{\ln}} - \sigma\right). \tag{9}$$

Substituting the derivatives of nominal stress and strain, $dF = A_o \cdot dT$, and $d\varepsilon_b = dL/L_o$, yields

$$\left(\frac{dT}{d\varepsilon_b}\right) \cdot \left(\frac{A_o}{L_o}\right) = \frac{A}{L}\left(\frac{d\sigma}{d\varepsilon_{\ln}} - \sigma\right). \tag{10}$$

The threshold of instability occurs when there is a zero tangent slope in the nominal stress/strain curve, hence

$$\text{instability threshold}: \quad \frac{dT}{d\varepsilon_b} = 0 \quad \rightarrow \quad \frac{d\sigma}{d\varepsilon_{\ln}} = \sigma \,. \tag{11}$$

Necking will continue as long as

$$\text{necking}: \quad \frac{dT}{d\varepsilon_b} < 0 \quad \rightarrow \quad \frac{d\sigma}{d\varepsilon_{\ln}} < \sigma \,. \tag{12}$$

When these derivatives are positive the deformation will be stable.

2.4 Obtaining plausible stress/strain material representation when materials exhibit local necking

The prior discussion and analysis provide formulae to determine what parts of the *apparent* nominal stress/strain curve of Figure 2e are valid and which are not. Moreover, we can also use these formulae to make several educated guesses of plausible forms for the stress/strain curve of the material during the states when the specimen was exhibiting local necking and neck propagation (between states A and B of Figure 2e).

Figure 4a presents four different assumed stress/strain curves to represent the material behavior of the Ö-Colamin film, as well as the apparent data from the physical experiment. Both nominal and true forms of the curves are shown, where mapping between the two forms is achieved via equations 1 – 4. These curves, labeled **A** – **D**, include a case for which the material should always remain stable (**A**), a marginally stable case (**B**), and two cases (**C** and **D**) where the material is defined to have inherent instabilities that should create necking. Case **D** is simply a direct use of the apparent stress/strain measured data from Figure 2e. Case **C** has no specific basis for its definition other than to be an unstable case. For the Ö-Colamin film that was experimentally tested, only cases **C** and **D** would be considered plausible, since they should produce an instabilty. Cases **A** and **B** are additional "sanity-checks" to ensure that they do *not* become unstable when utilized in a simulation.

To evaluate the plausibility of the four different stress/strain curves of Figure 4a, finite element models representing the uniaxial test depicted in Figures 1 and 2 were utilized. The models simulated rigid clamps at each end of the specimen and used plane stress 2D elements, type CPS4R. For all the cases analyzed, elastic/plastic material laws were used that were derived from the true stress/strain representations of Figure 4a. All cases used an elastic modulus of E_o = 605 MPa, Poisson's ratio of $\nu = 0.4$, and initial yield stress of 12.1 MPa (true stress). For each of the four material representations (**A** – **D**), plastic strain data for the `*PLASTIC` card was derived via

$$\varepsilon_{\ln}^{pl} = \varepsilon_{\ln} - \frac{\sigma}{E_o} \,, \tag{13}$$

where ε_{ln} is the total true strain for any given true stress σ.

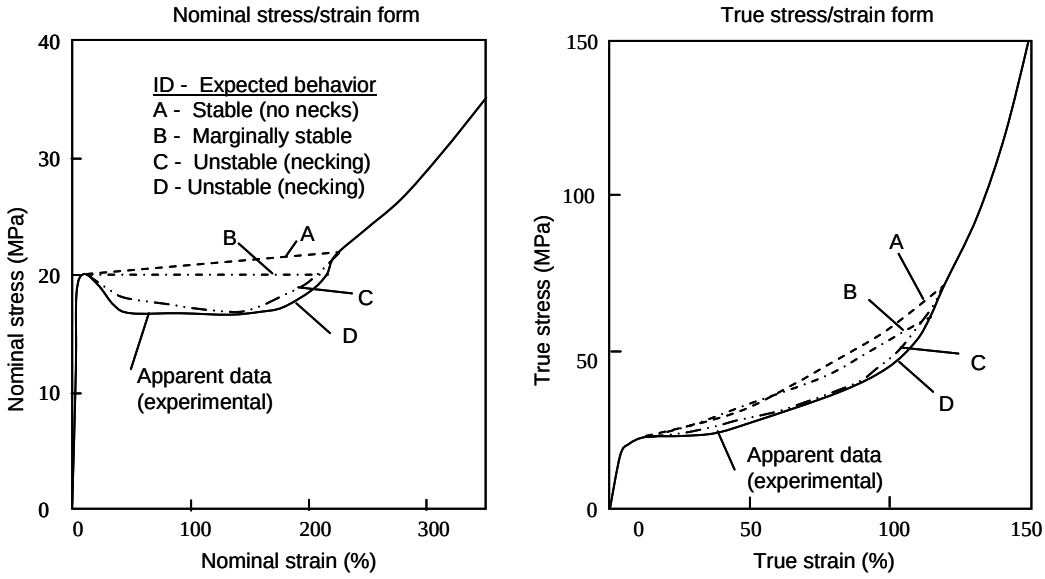

a) Stress/Strain curves used to generate *Elastic and *Plastic data for ABAQUS simulations

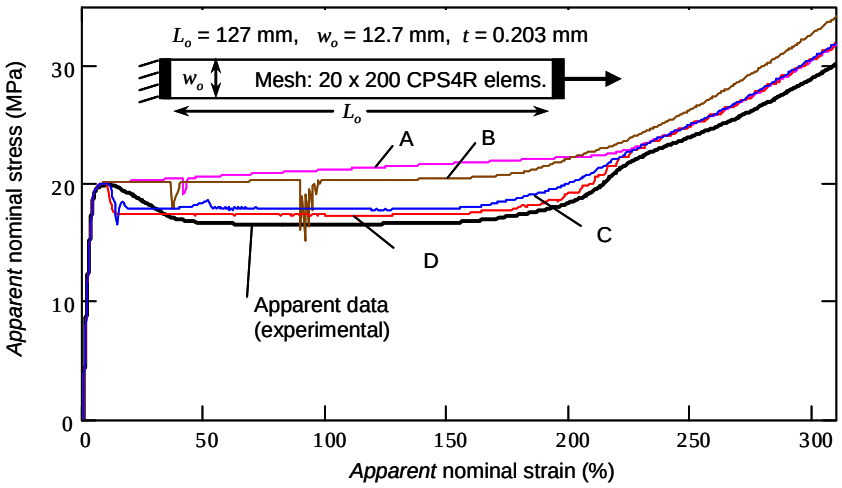

b) *Apparent* nominal stress/strain curves derived from ABAQUS/Explicit simulation data

Figure 4: Various forms of stress/strain curves evaluated with FE models.

Modeling unstable material definitions with nonlinear finite element methods is likely to cause convergence difficulties with implicit techniques, so initial analyses were done with ABAQUS/Explicit. These models were run using a prescribed velocity boundary condition that smoothly ramped the displacement over the duration of the simulation at a rate such that kinetic energy was sufficiently small to simulate quasi-static loading. All models used a volumetric mass density of 1.04 kg/m^3. No specific perturbations or defects were utilized in the models to entice necking to occur, except for the unstable material definitions themselves. It was expected that the strain wave propagation that naturally exists in an ABAQUS/Explicit model would be a sufficient perturbation. Also, because of the clamped boundary conditions on each end of the sample, a small strain gradient would exist to help initiate a localized neck (if the material definition contained instability).

Figure 4b presents the resulting *apparent* nominal stress/strain curves obtained from the ABAQUS/Explicit models along with the original experimental result. The *apparent* curves for the four cases were computed from the reaction force and displacement from the right-side boundary condition. All ABAQUS/Explicit history data utilized the built-in antialiasing filter feature with 700 points of output. Several conclusions can be drawn from the results.

The material definition that was intended to be stable (**A**) produced a stable result in the simulation. The marginally stable definition (**B**) also produced a stable result. There was no localized necking observed in either of these cases. The other cases, **C** and **D**, exhibited localized necking as expected. Figure 3 contains images of strain and stress contours from case **D**, clearly showing initiation of a localized neck and its propagation. Case **C** (not shown in Figure 3) also exhibited the same phenomenon, although the location where necking began and its actual propagation in the specimen were slightly different.

The resulting *apparent* nominal stress/strain data from cases **C** and **D** produced results similar to the physical experiment. Some limited assessments of variations from these material definitions were studied to see if a less abrupt drop in *apparent* nominal stress could be obtained in the simulation at the onset of necking, although no improvements were found. At this point it is suspected that viscous rate effects in the actual material, which were not present in the models studied, were the major cause for this discrepancy.

It is also noted that both cases **A** and **B** showed a short duration, high-frequency response between 30% and 100% apparent nominal strain. The antialias output filter of ABAQUS/Explicit partially masks this result, but the disturbance is still clearly seen in the data. This may be caused by the fact that both cases **A** and **B** actually have a nearly infinitesimal portion of their material definition which is marginally stable (at the initial peak of the nominal stress/strain curve around 10% strain; this is not easily seen in the figure).

Figure 5 presents the results of similar models that were run in ABAQUS/Standard. All the results depicted in this figure utilized the material definition from case **D** of Figure 4a. Using the default nonlinear static step controls (`Stabilize` option not used), the ABAQUS/Standard model terminated due to convergence problems at an apparent nominal strain of around 13% (Figure 5a). As expected, the implicit solver had difficulty with the unstable material law definition. Using the default settings for `Stabilize` (dissipated energy fraction of 2.0e-4, Figure 5a), a neck clearly

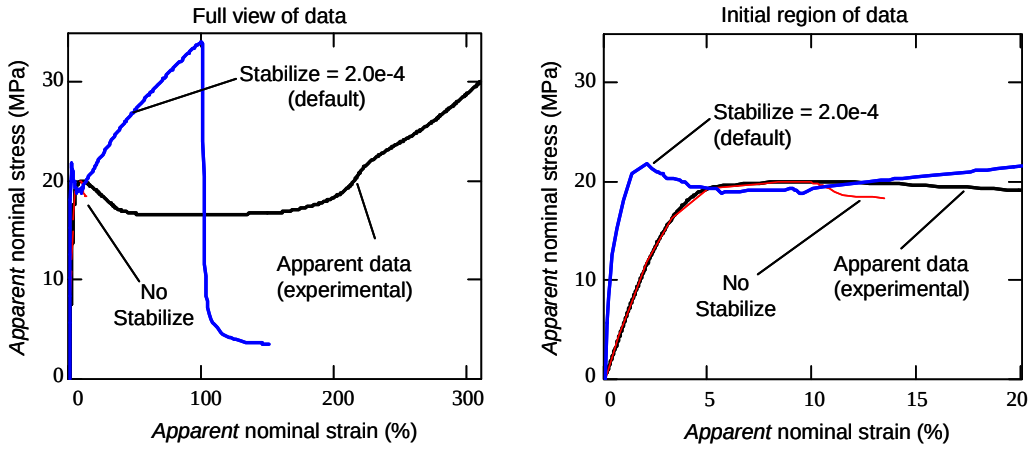

a) Results derived from ABAQUS/Standard V6.6 simulation data without stabilization and with stabilization (using default parameter value).

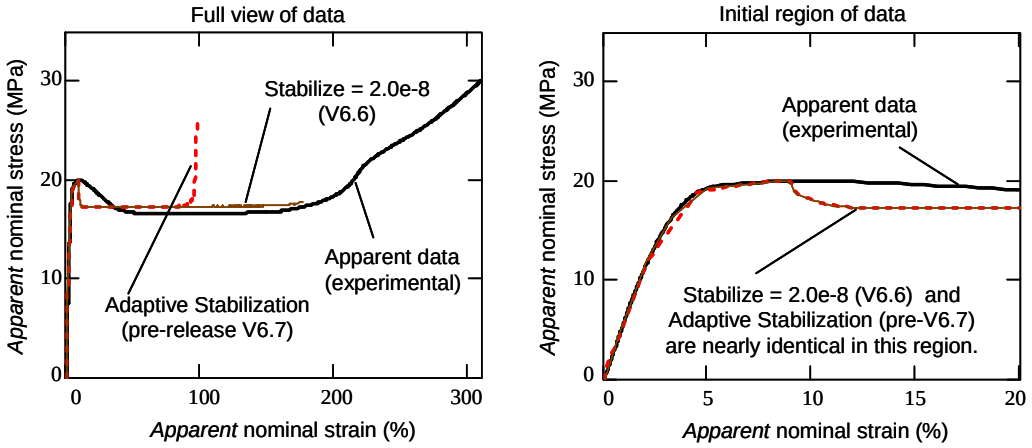

b) Results derived from ABAQUS/Standard V6.6 simulation data using non-default stabilization parameter value and from ABAQUS/Standard V6.7 pre-release using new adaptive stabilization algorithm.

Figure 5: Solutions obtained with ABAQUS/Standard for models defined with the unstable material definition "D" from Figure 4a.

developed and propagated for a large distance before the solution terminated due to extremely large strain in one element. Unfortunately, the default stabilization energy significantly distorted the solution as shown in the *apparent* nominal stress/strain curve of Figure 5a. More disturbing was the observation that this distortion existed from the beginning of the analysis, even in the elastic regime where no plastic deformation had yet occurred and no material instability had yet been encountered. Evaluation of damping energy ALLSD (not plotted here) for this case showed that the default stabilization value created artificial damping that was significant, similar in magnitude to the strain energy ALLIE in the model.

Reduction of the dissipated energy fraction for stabilization by a factor of 10 to 2.0e-5 (not plotted here) showed negligible improvement in the result. However, when the dissipated energy fraction for stabilization was set at 2.0e-8 (4 orders of magnitude less than the default), the model performed much better (Figure 5b). For this case, the apparent nominal stress/strain curve was more accurate. Also, the damping energy ALLSD was very small compared to ALLIE. The localized necking behavior and propagation for this case was also very close to the predictions from ABAQUS/Explicit. It is noted, however, that this ABAQUS/Standard simulation still terminated prematurely due to convergence problems at an *apparent* nominal strain of approximately 180%.

One additional ABAQUS/Standard simulation was evaluated using a new adaptive stabilization algorithm that is being developed for ABAQUS V6.7. Figure 5b presents these results computed with a pre-release version of ABAQUS V6.7. This adaptive algorithm, which does not require user specification of a dissipated energy fraction, performed very well until about 100% apparent nominal strain, at which point the solution diverges and terminates. Up to this point, damping energy ALLSD was very small compared to ALLIE.

It is important to re-emphasize that attempting to model such an unstable material law with any implicit FE code (ABAQUS/Standard in this case) is traditionally not recommended and known to be extremely challenging. Nonetheless, some level of success can be achieved, albeit with a bit of effort and caution. Clearly though, an explicit dynamics solution algorithm such as ABAQUS/Explicit is better suited for this type of unstable material model.

3. Implications on biaxial loading

This section presents some initial evaluations for biaxial loading of unstable materials. Figures 6 and 7 show the results of ABAQUS/Explicit simulations for two different biaxial loading conditions. In both simulations, the material representation used is from case **D** of Figure 4a. The simulations point out some interesting results that are obtained because of the combination of an unstable material behavior, geometry, and loading.

The cruciform simulation of Figure 6 predicts that, for the material analyzed, it would be impossible to obtain very large inelastic deformation in the biaxially-loaded portion (center of cruciform) of the specimen. Figure 6b predicts that during initial loading of the cruciform the uniaxially-loaded arms will exhibit localized necking. This is caused by the fact that the mises

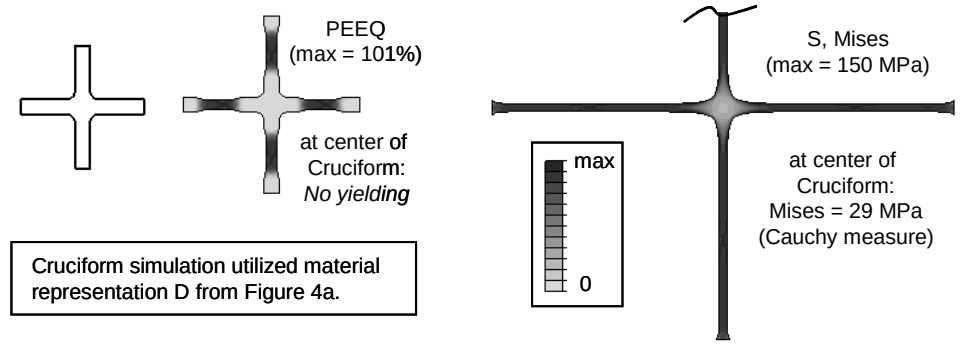

Figure 6: ABAQUS/explicit predictions of biaxial response for cruciform loading.

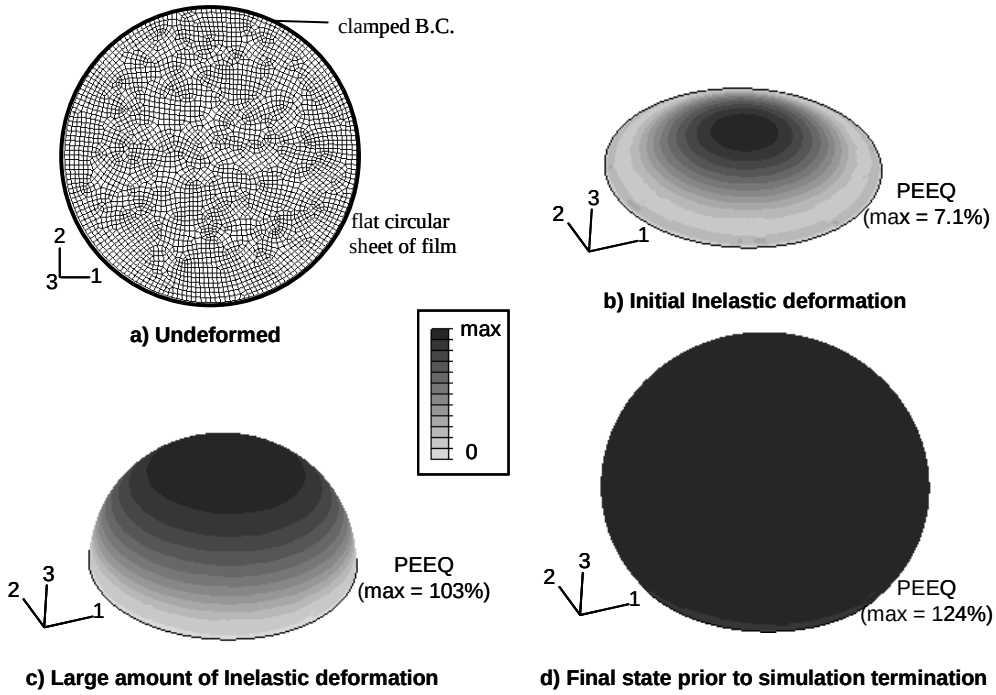

Figure 7: ABAQUS/explicit predictions of inflation of a flat circular sheet utilized material representation D from Figure 4a.

stress during elastic loading is larger in the uniaxially-loaded arms than in the biaxially-loaded center of the cruciform. Even after the localized necking has been arrested in the cruciform arms, the arms continue to uniformly neck as the center portion of the cruciform begins to experience modest inelastic deformation. Ultimately the simulation terminates when the arms' strain exceed the maximum defined inelastic strain (failure strain) prescribed on the `*PLASTIC` material card. In the cruciform analysis, the center only experienced a maximum true stress of 29 MPa. This equates to an inelastic strain, PEEQ, of 53% (true strain), which is significantly less than the material's failure value of inelastic strain, 124% (true strain).

The inflation simulation of a flat circular sheet presented in Figure 7 demonstrates that this type of geometry and loading produces a very different response compared to the cruciform. Throughout the entire loading history, as the inflation pressure is increased (up to failure), the maximum strains and stresses exist at the center of the sheet. This is the location where the material is exhibiting equibiaxial deformation. As shown in the simulation, this type of loading enables the material to be biaxially loaded to the point of material failure.

This inflation test also enables the possibility of experimentally measuring both biaxial strains and biaxial stresses. Using membrane theory, the local stresses in the inflated sheet are related to the local curvature of the sheet and the sheet's deformed thickness. Using a non-contact digital image correlation method, a contour map of the sheet's deformed shape, local strains, and curvatures can be obtained from a physical experiment. This information would be sufficient to measure a complete biaxial stress/strain curve for the material. This is an important finding because such a complete result does not appear to be possible in a uniaxial testing configuration.

A final point about these biaxially loaded examples is that in neither case did the simulations predict that the deformation would become asymmetric. That is, none of the biaxial solutions indicated that a localized neck would form in a given direction. It is possible that this behavior did not occur because 1) an initially isotropic material law definition was utilized, 2) there was not a sufficiently large perturbation, or 3) the predictions of symmetric deformations are correct. At the time of this writing, such a physical test has not been performed on the Ö-Colamin material.

4. Conclusions

This study presented a method to obtain plausible material law representations for materials that exhibit significant localized necking during large-strain uniaxial deformations. The work presented conditions that defined regions of stability and instability in terms of both nominal stress/strain and true stress/strain measures. It was demonstrated that even though an experimentally measured *apparent* nominal stress/strain curve was technically invalid after the onset of localized necking, that such a curve could still be used to create a plausible material law. The stability conditions provided further guidance for obtaining plausible material representations. The study also demonstrated the robustness of the explicit dynamics solution method for such unstable materials. Implicit solutions were also demonstrated, but they were less robust and more difficult to obtain for all cases studied. The analysis also evaluated two biaxial loading states and predicted that a classic cruciform test is unlikely to be able to create sufficiently large strains in the biaxially-loaded center portion before failure of the cruciform arms occurs. Results from inflation

of a flat circular sheet were more favorable and indicated that the sheet's center could withstand biaxial loading up to the point of material failure. It was also suggested that this circular sheet inflation test configuration allowed for the possibility of obtaining physical measurement data for both the material's strain and stress using non-contact digital image correlation methods.

5. References

1. ABAQUS, *ABAQUS Version 6.6 Documentation*, ABAQUS, Inc., 2006.
2. ABAQUS, *Metal Inelasticity in ABAQUS*, course notes, ABAQUS, Inc., 1996.
3. Obermühle Polymertechnik, manufacture of Ö-Colamin "MP" Flachfolie film, Püßneck, Germany.

6. Acknowledgment

The author wishes to acknowledge the support of DuPont colleagues Leo Carbajal, Jay Sloan, William Coulter, Clifford Deakyne, David Roberts, Patrick Young, and Mark A. Lamontia. The interactions with Dale Berry and others at ABAQUS are also acknowledged. Their support and technical interactions over the duration of this project are greatly appreciated.